Intrusion and extrusion of a liquid on nanostructured surfaces

M. Amabili,[1] A. Giacomello,[1] S. Meloni,[1] and C.M. Casciola[1]

[1]*Sapienza Università di Roma, Dipartimento di Ingegneria Meccanica e Aerospaziale, 00184 Rome, Italy*

arXiv:1702.00332v1 [cond-mat.mes-hall] 1 Feb 2017

Abstract

Superhydrophobicity is connected to the presence of gas pockets within surface asperities. Upon increasing the pressure this "suspended" state may collapse, causing the complete wetting of the rough surface. In order to quantitatively characterize this process on nanostructured surfaces, we perform rare-event atomistic simulations at different pressures and for several texture geometries. Such approach allows us to identify for each pressure the stable and metastable states and the free energy barriers separating them. Results show that, by starting from the superhydrophobic state and increasing the pressure, the suspended state abruptly collapses at a critical intrusion pressure. If the pressure is subsequently decreased, the system remains trapped in the metastable state corresponding to the wet surface. The liquid can be extruded from the nanostructures only at very negative pressures, by reaching the critical extrusion pressure (spinodal for the confined liquid). The intrusion and extrusion curves form a hysteresis cycle determined by the large free energy barriers separating the suspended and wet state. These barriers, which grow very quickly for pressures departing from the intrusion/extrusion pressure, are shown to strongly depend on the texture geometry.

I. INTRODUCTION

Since the seminal papers of Wenzel in 1936 [1] and of Cassie and Baxter in 1944 [2] it is known that surface roughness can be used as a means to control the wetting properties of a surface. On hydrophobic surfaces, capillarity allows for sustaining a liquid-vapor interface atop surface asperities; this is the so-called Cassie state which gives rise to superhydrophobic properties [3]. In the last decade, due to the rapid improvement in the nano-fabrication techniques [4], the field is experiencing a renewed interest both for technological applications [5, 6] and more fundamental studies [7, 8]. Among other possible applications, superhydrophobicity is of paramount importance in submerged conditions for its capability to enhance slip [9, 10] and thus reducing drag [11]. However, in addition to the Cassie state, the liquid can assume other states, e.g., by fully wetting the surface roughness [12]: this is the Wenzel state [1] in which superhydrophobic properties are lost.

Stability of the Cassie state in submerged conditions has been tested experimentally by several groups [13–16]. Checco et al. [14] studied the collapse of the superhydrophobic state for surface textures of ca. 20 nm with different geometries via intrusion/extrusion experiments at isothermal conditions. The experiment measured via small angle x-ray scattering the *volume fraction* occupied by the vapor confined within the nanostructures as a function of the applied pressure. The experiment showed that, for hydrophobic nanotextures, the intrusion/extrusion cycle is characterized by a strongly hysteretic behavior. More in detail, during the intrusion process, the Cassie state is stable up to a critical pressure at which the liquid abruptly fill in the surface nano structure, i.e., the system falls in the Wenzel state. While in the extrusion process, when the pressure is reduced down to the initial conditions, the liquid cannot escape from the cavity; the transition to the Wenzel state is thus irreversible (at least at positive pressures). The authors also show that the stability of the Cassie state crucially depends on the geometry of the surface. A similar hysteretic behavior was also found for the wetting/drying of nanopores [17–19]. In particular, Lefevre et al. [17] used macroscopic capillarity theory and line tension effect to understand the hysteresis. This theory predicts that hysteresis should vanish if the pore dimension is of the order of 2 nm; at this scale, however, the macroscopic theory may become unsuitable for describing the system. Similar hysteretic behaviors are common in the neighboring field of porous materials [20, 21] in which, for example, the intrusion/extrusion curves of mercury

are used as a means to characterize the pore structure [22]. At the origin of these experimental evidences of hysteresis in the intrusion of a liquid in nanostructured or porous surfaces is the presence of strong metastabilities; however, the microscopic aspects and the dependence on the surface geometry are not clearly understood and call for additional investigations. Explaining these aspects is crucial in order to define reliable design criteria that could help the engineering of superhydrophobic surfaces. In particular, an important goal is to improve the stability of the Cassie state [23, 24] or to favor the recovery of superhydrophobicity from the Wenzel states [8].

Since the wetting properties of textured surfaces on the nanometer scale are difficult to access experimentally, in this work molecular dynamics (MD) simulations are performed with the aim of reproducing a nanoscale intrusion/extrusion experiment. The investigated surface, reported in Fig. 1a, is characterized by a re-entrant T-shaped cavity inspired by experimentally reproducible surfaces which show superhydrophobic behavior even to low surface tension liquids [5, 25] (omniphobicity).

In addition, at the nanoscale, thermal fluctuations could play a role in triggering the transition from Cassie to Wenzel: when the free energy barriers separating the two states are of the order of k_BT, with T the temperature and k_B the Boltzmann constant, they can be overcome with the aid of thermal fluctuations. The kinetics of this transition exponentially depends on the ratio between the value of the free-energy barrier and on the thermal energy available to the system k_BT (see eq. 4 below). Thus when the barriers are large as compared to k_BT the transition is a *rare event* meaning that happens on very long timescale. Here, in order to assess in terms of free energy the stability of the Cassie state and to interpret in quantitative terms the intrusion/extrusion results, a rare event MD method is employed – the Restrained MD [26]. This technique allows one to compute the free-energy profile connected to the Cassie-Wenzel transition and thus to characterize the metastable states the barriers separating them.

In summary, the aim of this work is to study the wetting properties of a T-shaped, structured surface of nanometer size. First an *in silico* intrusion/extrusion experiment is performed. Then the ensuing hysteresis cycle is interpreted thanks to additional rare event simulations aimed at quantifying the free energy barriers. The present simulations also yield insights into the irreversibility of the Cassie breakdown.

The paper is organized as follows. In section II the details of the MD intrusion/extrusion

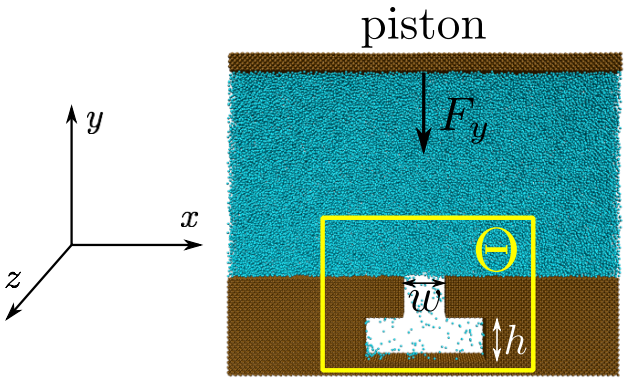

FIG. 1. Sketch of the atomistic system. The fluid and solid particles are represented in blue and brown, respectively. The yellow box corresponds to the control region used for the definition of $\Theta(\mathbf{r})$.

experiment and of the restrained MD method are reported. Results are consecutively discussed in section III, while the conclusions are drawn in the last section.

II. METHODS

The system consists of a fluid enclosed between two solid walls. The bottom solid wall is decorated with a T-shaped nanocavity while the upper one is planar and acts as a piston on the system (Fig. 1). Fluid particles interact via the standard Lennard-Jones (LJ) potential, while solid and fluid particles interact with the following modified LJ potential [27]:

$$V^{\mathrm{sf}}(r) = 4\epsilon \left[\left(\frac{\sigma}{r}\right)^{12} - c \left(\frac{\sigma}{r}\right)^{6} \right] \tag{1}$$

where ϵ and σ are the standard LJ parameters and r is the inter-atomic distance between a solid and a fluid particle. The parameter c modulates the attractive component in eq. 1, which effectively tunes the chemistry of the surface. Here a hydrophobic surface is considered with $c = 0.6$. The ensuing chemistry of the surface is evaluated by computing the Young contact angle θ_Y of a sessile cylindrical drop deposited on a flat surface. This measure has been performed in our previous work yielding $\theta_Y \simeq 110^\circ$ [28, 29]. In order to produce quantities which are directly comparable with experiments, the results are converted in SI units using the LJ parameters of Argon, i.e., $\sigma = 0.3405$ nm and $\epsilon/k_B = 119.8$ K [30]. Fluid particles are kept at constant temperature $T = 95.8$ K using a Nosé-Hoover chain thermostat [31].

First, an intrusion/extrusion molecular dynamics "experiment" is performed on the system in Fig. 1. In order to obtain the pressure against filling diagram, which is also the final outcome of actual experiments [13, 14], two main aspects need to be addressed: i) characterize the thermodynamic conditions of the system; ii) compute the vapor fraction ϕ_v within the nanocavity, e.g., by counting the number of particles in a region enclosing the surface texture (see Fig. 1).

Concerning i), the temperature is fixed by the thermostat while the pressure difference $\Delta P = P_l - P_v$ between the liquid and vapor phases can be computed. In particular, P_l is controlled by means of the upper solid wall acting as a piston; a constant force F_y is applied in the y direction to each particle of the upper wall. In the steady state, the total piston force is balanced by the liquid pressure $P_l = F_y N_w / A$ where N_w and A are the number of particles and the surface area of the piston, respectively (see also the *Supplementary Data*). This means that imposing F_y is equivalent to control P_l. The vapor pressure depends mainly on T and has been computed in a previous work: $P_v = 0.35$ MPa at $T = 95.8$ K [29]. The piston is employed here instead of other "bulk" barostats in order to avoid problems arising from the presence of (changing) interfaces; this approach ensures that ΔP has a constant value along the transition which can be thus compared with experiments (see the *Supplementary Data*).

Concerning ii), in a liquid-vapor biphasic system, the void fraction ϕ_v can be computed by defining the observable $\Theta(\mathbf{r})$ which counts the number of fluid particles in the yellow box of Fig. 1, with $\mathbf{r} = (\mathbf{r}_1, ..., \mathbf{r}_N)$ the coordinates of the N fluid particles. Thus ϕ_v is computed via the following relation:

$$\phi_v \equiv \frac{\overline{\Theta(\mathbf{r})} - N_W}{N_C - N_W} \tag{2}$$

Where N_C and N_W are the number of particles in the Cassie and Wenzel state at $\Delta P = 0$, respectively and $\overline{\Theta(\mathbf{r})}$ denotes the time average.

From the definition in eq. 2 it follows that $\phi_v \approx 1$ corresponds to the Cassie state, while $\phi_v \approx 0$ to the fully wet Wenzel state.

In Sec. III the results of the intrusion and extrusion MD simulation are presented just as the outcome of an experiment. Additionally, on the very same system *rare event* simulations are performed, which give access to the free-energy profiles and barriers, to the transition kinetics, and to the multiple (meta)stable states. Such additional simulations are useful to

interpret the experimental results and, in particular, the strong hysteresis encountered in strongly metastable systems. A rare event is a process that happens with a frequency which is too low as compared to the typical simulation time (several hundreds ns up to μs) to obtain statistical information via *brute force* techniques.

Here the transition is described in terms of a single collective variable, the number of particles $\Theta(\mathbf{r})$ inside the yellow region in Fig. 1. In principle relevant information about the kinetics of the transition can be extracted by computing the probability that $\Theta(\mathbf{r})$ assumes a given value N_{box}, $p(\Theta(\mathbf{r}) = N_{box}) \equiv p_\Theta(N_{box})$. Given $p_\Theta(N_{box})$, the Landau free energy is defined as:

$$\Omega(N_{box}) = -k_B T \ln p_\Theta(N_{box}) \; . \tag{3}$$

Metastable states are the minima of $\Omega(N_{box})$, which correspond to high probability regions of the phase space; the free-energy maxima are known as transition states. The free-energy difference between a minimum and the neighboring maximum define a free-energy barrier $\Delta\Omega$ which, in turn, dictates the kinetics of the transition via

$$t = t_0 \exp\left(\Delta\Omega/(k_B T)\right) \; , \tag{4}$$

where t_0 is a prefactor and t is the average time needed to observe a transition. In other words, t defines the average lifetime of a stable (absolute free energy minima) or metastable (relative free-energy minima) state.

As mentioned above, $\Omega(N_{box})$ cannot be computed by brute force simulations due to the infrequent transitions between metastable states (see eq. 4) which prevents one to compute $p_\Theta(N_{box})$ directly. Here we employ Restrained Molecular Dynamics (RMD) in order to overcome the rare event issue and reconstruct $\Omega(N_{box})$. In RMD the physical potential (eq. 1) is augmented by a *restraining* potential of the form $V_{umb}(\mathbf{r}) = k/2 \; (\Theta(\mathbf{r}) - N_{box})^2$. This potential, for suitably large values of the constant k, restrains the system close to the condition $\Theta(\mathbf{r}) = N_{box}$ allowing one to sample regions of the phase space with low probability, which are not accessible to standard MD (see eq. 3).

The key quantity to compute in RMD is the free-energy gradient $\mathrm{d}\Omega/\mathrm{d}N_{box}$ from which by a simple integration $\Omega(N_{box})$ can be reconstructed. In particular, it is possible to demonstrate that $\mathrm{d}\Omega/\mathrm{d}N_{box}$ can be estimated via the time average of the mean force of the biasing potential [26]:

$$\frac{\mathrm{d}\Omega}{\mathrm{d}N_{box}} \approx \frac{1}{\tau} \int_0^\tau -k \left(\Theta(\mathbf{r}(s) - N_{box})\right) \mathrm{d}s \tag{5}$$

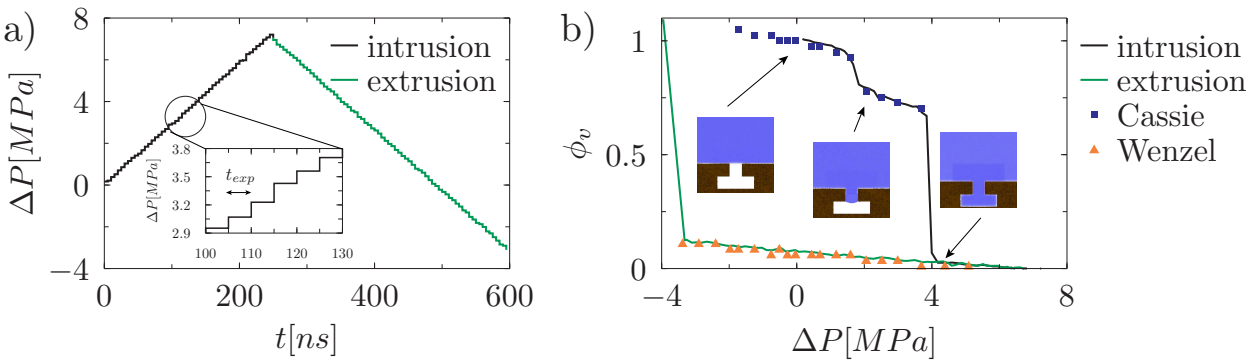

FIG. 2. a) Pressure signal applied to the system as a function of time during the MD "experiment"; the inset shows a magnification. b) Vapor fraction ϕ_v as a function of the applied ΔP evaluated during the experiment (black and green lines). The insets show the observed system configurations. The orange and blue symbols are the location of the free-energy minima corresponding to Wenzel and Cassie states, respectively.

where the time average is computed along the RMD of duration τ. In practice, the right-hand-side of eq. 5 is computed on a set of N^i_{box} fixed points via independent RMD simulations, from which the free-energy gradient is numerically integrated to reconstruct $\Omega(N_{box})$. Because of the linear relation between N_{box} and ϕ_v, from $\Omega(N_{box})$ one can easily obtain $\Omega(\phi_v)$, which will be used in the next section .

Simulations are performed with the open source code LAMMPS [32]. Furthermore, to perform RMD simulations LAMMPS is combined with the PLUMED tool for rare event computations [33].

III. RESULTS AND DISCUSSION

A. An MD "experiment"

In the following a T-shaped geometry with $w = 3.4$ nm and $h = 4.5$ nm is investigated (Fig. 1). The intrusion MD experiment starts in the Cassie state and at conditions close to two-phase coexistence $\Delta P \approx 0$ and consists in gradually increasing the pressure ΔP up to a large positive value ΔP_{max}, which is sufficient to trigger a spontaneous transition to the Wenzel state. When this stage is reached, ΔP is decreased until low negative pressures ΔP_{min} are achieved (extrusion process). In practice, a staircase pressure signal is applied

to the system (see Fig. 2a). The total pressure cycle lasts 600 ns; every $t_{exp} = 5$ ns, ΔP is increased (or decreased). After a certain force is suddenly imposed to the piston, the system equilibrates to the new ΔP in a time $t_{st} = 1$ ns (see the *Supplementary Data*). During the pressure cycle, for each value of ΔP the vapor fraction ϕ_v is computed; the final outcome of this "experiment" is plotted in Fig. 2b.

At $\Delta P \approx 0$, at the beginning of the experiments, the system is in the Cassie state, which is the stable state at the given thermodynamic conditions (see the next Section). As the pressure is increased, for $\Delta P < 2$ MPa, the system remains in the Cassie state with the liquid-vapor interface pinned at the outer corner of the cavity. ϕ_v marginally varies with ΔP, due to the increasing curvature of the pinned meniscus [34]. At $\Delta P \approx 2$ MPa a sharp transition is observed and the vapor fraction drops to $\phi_v \approx 0.75$. There the liquid-vapor meniscus is pinned at the inner corner of the T-shaped geometry; this second Cassie state, called inner-Cassie in the following, is shown in Fig. 2b. This behavior explains why the re-entrant geometry allows for stabilizing the vapor bubble for an additional range of pressures which would be impossible to achieve with straight walls [24]. A second transition is observed at $\Delta P \approx 4$ MPa, where the Wenzel state is eventually reached at $\phi_v \approx 0$: this is the critical intrusion pressure ΔP^C_{sp}. The macroscopic Laplace law predicts that $\Delta P^C_{sp} = 2\gamma_{lv}/w$, where γ_{lv} is the liquid-vapor surface tension. In the same conditions the macroscopic prescription $\Delta P^C_{sp} = 3.98$ MPa is in remarkable agreement with the nanoscale case. Since the liquid incompressible, a further increase of the ΔP up to ≈ 5 MPa produces no significant changes in ϕ_v.

From this final configuration the extrusion stage begins and the pressure ΔP is gradually decreased. During the extrusion, the system does not follow the same path of the intrusion, thus creating a hysteretic cycle. From the Wenzel state it is impossible to recover the superhydrophobic Cassie state even when extremely low negative pressures of the order of $\Delta P \approx -3.5$ MPa are reached. In even more extreme tensile conditions, however, a new transition is observed. The system does not return back to the Cassie state but an unstable bubble forms, which rapidly grows leading to a sudden expansion of the simulations box, and to the vaporization of the liquid. This process is the confined counterpart of the usual liquid-to-vapor spinodal transition. As a consequence, once the system is in the Wenzel state, superhydrophobicity is lost and not even at low negative pressures Cassie state can be recovered.

ΔP range [MPa]	**Cassie**	**inner-Cassie**	**Wenzel**
$\Delta P > 4.0$			✓
$2.0 < \Delta P < 4.0$		✓	✓
$-2.0 < \Delta P < 2.0$	✓		✓
$-3.5 < \Delta P < -2.0$			✓
$\Delta P < -3.5$			

TABLE I. Stable and metastable states at a given pressure; the ✓symbol indicates the existence of the corresponding state.

The intrusion/extrusion MD experiment has two important features: 1) a strongly hysteretic behavior, similar to that found in actual experiments also for surface textures at the nanoscale [14]; 2) the presence of multiple metastable states, i.e., the Cassie, inner-Cassie state, and the Wenzel state. In order to understand why hysteresis emerges, in the following, we perform free-energy calculations, which additionally allow us to characterize the metastable states. This equilibrium approach can explain the non-equilibrium "experiment" only if the transformation is quasi-static. Three different timescales are present in our experiment. The first timescale is t_{st}, defined as the molecular timescale needed to the system to reach the *st*ationarity after a sudden ΔP change. The second timescale is t_{exp} which is the duration of a pressure step in the *exp*eriment. The third one is set by the activated kinetics of eq. 4, which determines the lifetime of the stable and metastable states. In particular, the relevant timescale is t_{eq} which is defined as the time to reach the thermodynamically stable (or *eq*uilibrium) state from a metastable state. Our calculations indeed show that for the present case the following inequality holds $t_{eq} \gg t_{exp} \gg t_{st}$ apart from a narrow pressure region very close to the transitions (see Figs. 2 and 3c). In these conditions one can safely assume that the intrusion/extrusion experiment is quasi-static and therefore it can be interpreted using the free-energy arguments.

B. Free-energy calculations

The free-energy profile as a function of ϕ_v is computed at different ΔP (Fig. 3a). The free energy profiles give access to the transition rate via eq. 4 and to the relative probability of any two states, e.g., Cassie and Wenzel via $P_C/P_W = \exp\left((\Omega_W - \Omega_C)/k_B T\right)$, where Ω_W

and Ω_C are the free energy of Wenzel and Cassie state, respectively. This allows one to define the stable (more probable) and the metastable (less probable) states at varying of the thermodynamic conditions. Depending on ΔP, the profiles show different sets of minima (see orange and blue symbols in Fig. 3a) which are collected in Table I. It is found that the Cassie and inner-Cassie states never exist in the same pressure range; elsewhere it was shown that this mutual exclusion is due to the geometry of the re-entrant cavity which allows for pinning at the upper and lower corners in non-overlapping pressure ranges [24]. Therefore in the following the two *suspended* states will be generically referred to as "Cassie".

The kinetics of the Cassie-Wenzel and Wenzel-Cassie transition are characterized by the free-energy barriers $\Delta\Omega_{CW}$ and $\Delta\Omega_{WC}$, respectively (Fig. 3b). The barriers are very large as compared to the thermal energy k_BT. Indeed assuming a conservative molecular time scale for the prefactor $t_0 = 10^{-15}$ s in eq. 4 and considering that, apart from very close to the transition pressure, the barriers are typically larger than 100 k_BT, it is possible to conclude that the lifetime of both stable and metastable state dictated by eq. 4 are large as compared to any other timescale in the problem (t_{exp} and t_{st}). This last observation allows us to confirm our quasi-static assumption made above.

Figure 3b allows one also to compute the coexisting pressure $\Delta P_{coex} \approx 1.8$ MPa, i.e., the pressure for which $\Delta\Omega_{CW} = \Delta\Omega_{WC}$ or analogously $\Omega_C = \Omega_W$. Thus Cassie state is the most probable state for $\Delta P < \Delta P_{coex}$, while Wenzel state is the absolute minimum for $\Delta P > \Delta P_{coex}$. For large positive pressures the Cassie minimum disappears and $\Delta\Omega_{CW} \to 0$: this pressure defines the *spinodal* conditions for the Cassie minimum, $\Delta P_{sp}^{C} \approx 4.0$ MPa, i.e., the limit for the mechanical destabilization of the superhydrophobic state. Instead, the pressure at which $\Delta\Omega_{WC} \to 0$ is known as confined liquid *spinodal*, $\Delta P_{sp}^{liq} \approx -3.5$ MPa, below which the Wenzel state does not exists anymore and the confined liquid becomes mechanically unstable.

Now it is possible to directly interpret the MD "experiment" with the equilibrium picture emerging from free-energy calculations. The free-energy profiles and barriers in Fig. 3 indeed confirm that, at $\Delta P \approx 0$, the Cassie state is thermodynamically stable. As the pressure is increased in the experiment, the system passes through a series of states which coincide with the Cassie free-energy minima at the related pressure (blue squares in Fig. 2b). For $\Delta P > \Delta P_{coex}$ the Cassie state becomes metastable. However, the barrier between the two states is still large as compared to the thermal energy causing $t_{eq} \gg t_{exp}$. In other words,

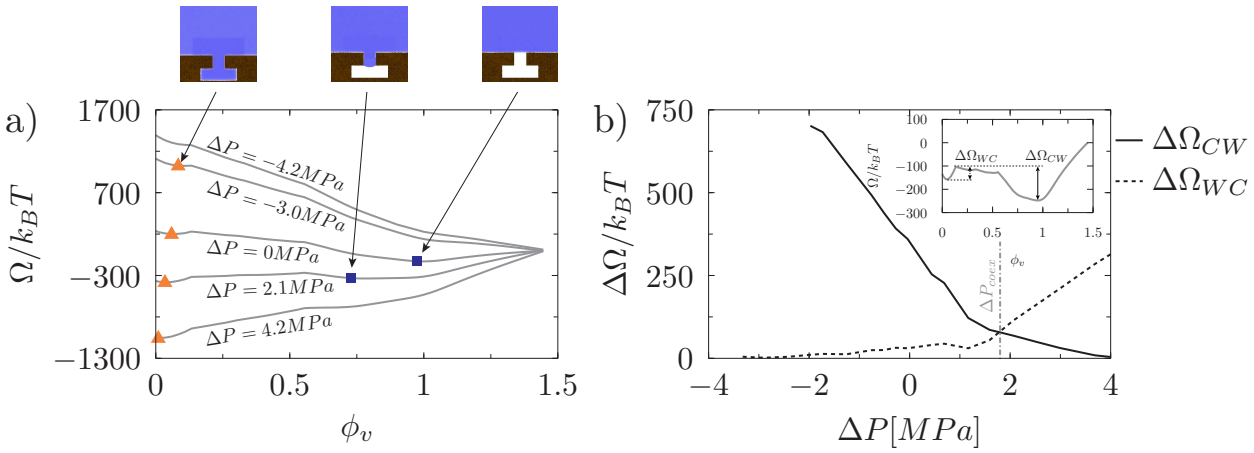

FIG. 3. a) Free-energy profiles at different ΔP (grey lines). The blue and orange symbols are the location of the minima corresponding to Cassie and Wenzel states, respectively. The insets show the mean density field in these states. b) Cassie-Wenzel and Wenzel-Cassie free-energy barriers as a function of ΔP. The definition of $\Delta\Omega_{WC}$ and $\Delta\Omega_{CW}$ are reported in the inset, showing the free-energy profile for a representative profile.

the experiment in not long enough to allow to the system to reach the absolute minimum of the free-energy, i.e., the Wenzel state. Indeed, in the experiment the transition to the Wenzel state happens only when $t_{eq} \leq t_{exp}$, i.e., when ΔP approaches the Cassie spinodal ΔP_{sp}^{C}.

During the extrusion stage, which consists in decreasing the pressure starting from the Wenzel state, the Cassie state cannot be recovered. This is due to the nucleation barrier $\Delta\Omega_{WC}$ which is never negligible up to very negative pressures preventing the system from undergoing a transition to the Cassie state (Fig. 3). In order to obtain again the Cassie state, one needs in principle to reach very large negative ΔP, i.e., the (confined) liquid spinodal ΔP_{sp}^{liq}. However, free-energy profiles show that the Cassie state exists in the range $-2 < \Delta P < 4$ MPa, while the liquid spinodal is reached only at $\Delta P_{sp}^{liq} \approx -3.5$ MPa. In practice, thermal fluctuations are again insufficient to restore the Cassie state in experiments. To overcome this irreversibility of the Cassie-Wenzel transition it is possible to manipulate the free-energy profiles by acting on the surface chemistry [35] or on its geometry [8, 36]. Reference [24] showed that the range of pressures in which the Cassie state exists can be broadened to very large negative ΔP using a hydrophilic layer at the top of the solid surface. This strategy, inspired by the natural case of Salvinia molesta [37], can open the door to

engineering of artificial surfaces with the capability to restore superhydrophobicity [38].

In practical applications, the presence of air or other gases seems to promote an easier recovery of the Cassie state, see, e.g., [36]. On the one hand, for slow changes in P_l as compared to the diffusion time t_D of air in the liquid, the gas simply acts as an additional pressure term in $\Delta P = P_l - P_v - P_g$; this slightly reduces the absolute value of P_l required to reach spinodal conditions. On the other hand, when pressure variations are fast as compared to t_D, air bubbles effectively prevent the system to reach the Wenzel state; as soon as the pressure is decreased again, these (tiny) bubbles act as cavitation nuclei allowing for an immediate formation the Cassie state. In this second case, which is difficult to distinguish experimentally from the first, the apparent recovery is facilitated only because the Cassie-Wenzel transition is never accomplished.

In summary, free-energy calculations demonstrate that, even for *nanoscale* textures, the barriers are much larger than k_BT thus confirming that thermally activated transitions are actually rare; the transitions will be observed only for conditions very close to the spinodal. Our conclusion is based on the relatively short duration of the *in silico* experiment; in actual applications one should always verify whether the considered experimental time t_{exp} is larger than t_{eq} or not. As an example, for $t_{exp} \approx 1$ h when the barriers are larger than ca. 40 k_BT, thermally activated events become irrelevant.

In addition, Fig. 2b shows a fair agreement between the free energy calculations and the intrusion/extrusion curves of the *in silico* experiment, confirming that the quasi-static assumption is valid even for very rapid pressure changes. In such strongly metastable systems, the intrusion/extrusion experiment strongly depends on the initial system configuration, here the Cassie state. The same experiment started in the Wenzel state would have a completely different results from that of Fig. 2b. For actual textured surfaces, the state of the system could be mixed, with (isolated) cavities both in the Cassie and Wenzel states; in such cases the interpretation of the intrusion/extrusion curves should be made with particular care.

The chemistry of the solid also plays an important role in determining the characteristics of the intrusion/extrusion cycle, compare, e.g., the present results with the experiments on hydrophilic Alumina [21]. To address this issue we have computed the free energy profiles at various ΔP of an hydrophilic surface with $\theta_Y \approx 55^\circ$ [39] (Fig. 4a). In Fig. 4b we report the vapor fractions corresponding to stable and metastable states as a function of ΔP.

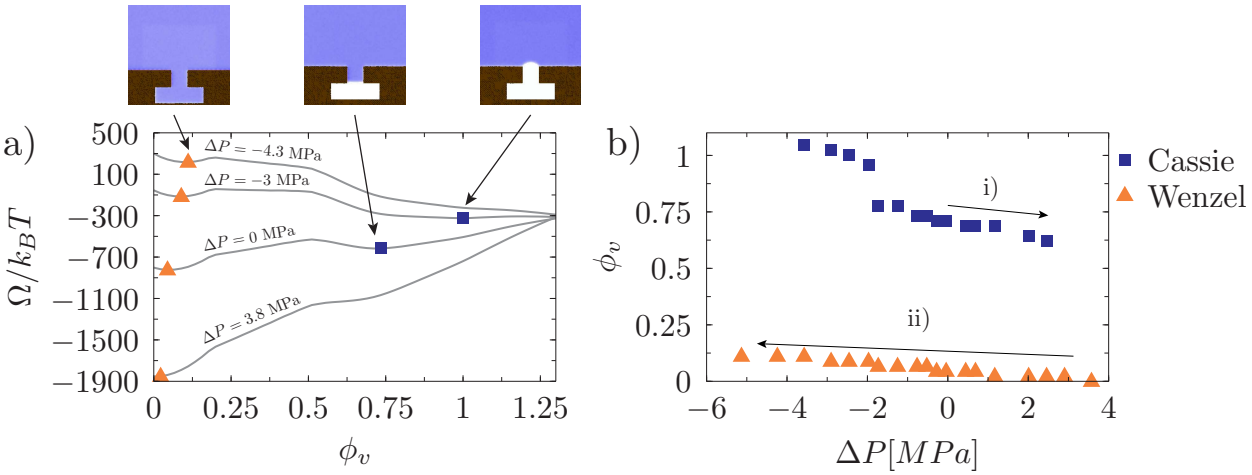

FIG. 4. a) Free-energy profiles for the hydrophilic chemistry ($\theta_Y \approx 55°$) at various ΔP. The insets show the system configurations of the stable and metastable states. b) Location of the metastable and stable states in the ϕ_v – ΔP diagram. The arrows indicate the result of a thought intrusion/extrusion experiment.

The system is still characterized by two Cassie (Cassie and inner-Cassie) and a Wenzel state. However, at variance with the hydrophobic case, in an intrusion experiment with initial pressure $\Delta P = 0$ MPa one would observe only the inner-Cassie to Wenzel transition ($\approx$ 3 MPa); furthermore for $\Delta P \geq 0$ the inner-Cassie state is always metastable. The usual Cassie state exists only for negative pressures (-4 MPa $\leq \Delta P \leq -2$ MPa). Finally, for the reentrant hydrophilic cavity the macroscopic estimate of the intrusion pressure via Laplace equation [29] yields $\Delta P^C_{sp} = 2\gamma_{lv} \sin\theta_Y / w = 3.26$ MPa, which is consistent with the atomistic value of 2.7 MPa. Like for the case of hydrophobic surfaces, the presence of a large free energy barrier prevents the reverse Wenzel to Cassie transition in the extrusion path, i.e. the system remains trapped in the wet state. It is worth remarking that for the hydrophilic surface the Wenzel state exists over an even larger range of negative pressures, at least up to the minimum value investigated in this work, $\Delta P = -6$ MPa.

C. Influence of the texture geometry

The previous results suggest that the intrusion/extrusion experiment critically depends on the characteristics of the nanotexture (see also Refs. [14, 36]). In the following, the geometry of the T-shaped cavity is modified in order to investigate how those features can

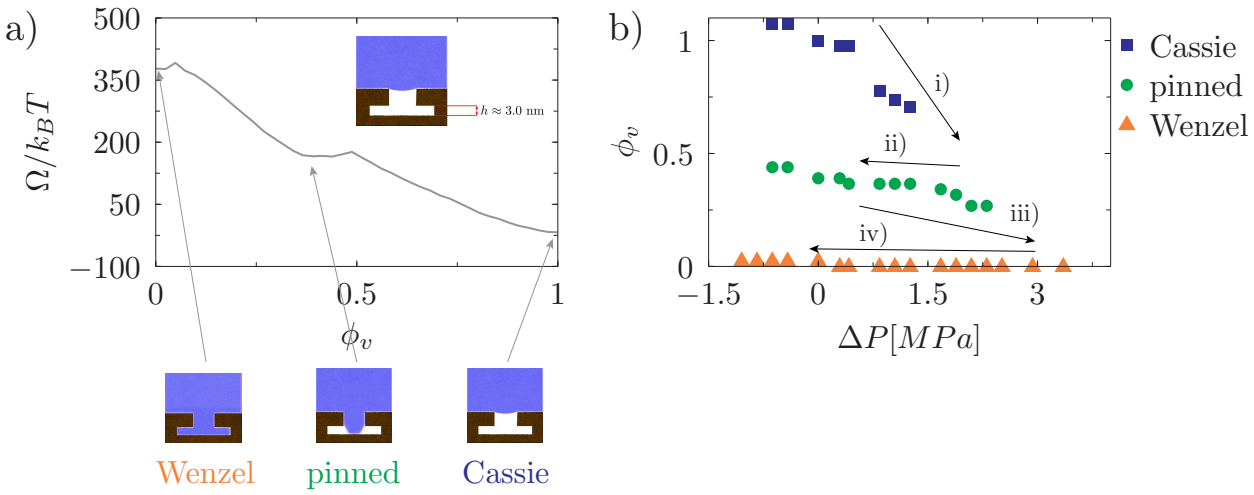

FIG. 5. a) Free-energy profile at $\Delta P \approx 0$ for the geometry shown in the inset. The bottom strip reports the configurations corresponding to the Cassie, pinned, and Wenzel states corresponding to the minima of the profile. b) Location of the three metastable states in the ϕ_v – ΔP plane as computed from free-energy profiles. Orange, green, and blue symbols correspond to Wenzel, pinned, and Cassie states, respectively. The arrows indicate the path followed in the thought intrusion/extrusion experiment discussed in points i)– iv) in the main text.

be tuned to obtain different stability properties for the Cassie state. Specifically, the new cavity has a larger cavity mouth $w \approx 9$ nm and is shorter, with a height $h \approx 3$ nm.

Figure 5a reports the free-energy profile at $\Delta P \approx 0$. Three minima are found: the usual Cassie and Wenzel states and a third one characterized by two liquid-vapor interfaces pinned at the inner corner of the structure and touching the bottom wall (in the following will be referred to as the *pinned* state). The vapor fraction of those states as a function of ΔP is reported in Fig. 5b which also shows the range of ΔP in which they exists. As for the previous geometry, depending on ΔP, two Cassie states are found, in which the bottom wall is not wet, one for $\phi_v \approx 1$ and one for $\phi_v \approx 0.75$ (inner Cassie). Due to the larger width of the cavity mouth, the Cassie spinodal pressure is lower than the previous case. Indeed, the macroscopic estimate for ΔP^C_{sp} based on Laplace law yields $\Delta P^C_{sp} = 2\gamma_{lv}/w$, where γ_{lv} is the liquid-vapor surface tension [24], thus to a larger w corresponds a lower ΔP^C_{sp}. Furthermore, Fig. 5b shows that the pinned state exist for a broader range of pressure as compared to that of the Cassie state.

The presence of a third *pinned* state may significantly alter the results of an intru-

sion/extrusion experiment. Starting from Cassie state, three transitions are expected along the intrusion process: from the Cassie to the inner-Cassie; from the inner-Cassie to the pinned state; from the pinned state to Wenzel. If the maximum applied pressure is sufficiently large to reach the Wenzel state the extrusion process is similar to the previous case in Fig. 2b, with a direct transition from the Wenzel to the vapor state. However, at lower maximum pressure more complex situations could arise. For instance, consider the following four step experiment:

1. starting from $\Delta P \approx 0$ MPa, increase the pressure up to $\Delta P \approx 2$ MPa;

2. decrease the pressure down to $\Delta P \approx 0$ MPa;

3. increase the pressure up to $\Delta P \approx 3$ MPa;

4. decrease the pressure down to $\Delta P \approx 0$ MPa;

The results of this thought experiment are reported in Fig. 5b with a dashed gray line. During step i), the system passes through the Cassie and inner-Cassie states and subsequently falls in the pinned state. In step ii), as the ΔP is decreased, the system remains trapped in the pinned state. As pressure is increased again up to $\Delta P > 2.5$ MPa in stage iii), the system undergoes a transition to the Wenzel state. Finally in stage iv) the system remains trapped in the Wenzel basin. A similar hysteretic behavior is found in Fig. 4 of Ref. [14], in which, however, the considered textures are not re-entrant. In this case the presence of defects at the nanoscale could give origin to multiple metastable states [40, 41] which can produce a hysteretic behavior similar to that described above.

IV. CONCLUSIONS

In this contribution an intrusion/extrusion molecular dynamics experiment has been performed on a surface decorated with T-shaped nanocavities. The pressure-filling diagram shows large hysteretic cycles; this phenomenon has been interpreted in terms of trapping of the system in different metastable states. Rare-event techniques allowed us to estimate the free-energy barriers and the relative probability between two (or more) metastable states. Results show that the Cassie-Wenzel and the Wenzel-Cassie transitions are characterized by

very large free-energy barriers also at the nanometer scale, which is difficult to access experimentally. The long kinetics connected with such barriers prescribes a well defined separation between the molecular, experimental, and thermodynamic equilibrium timescales. This separation has allowed us to interpret the MD experiment in terms of quasi-static process in which the system relaxes to the local minimum of the free energy (metastable state). Only close to the spinodal pressure, when the separation of timescales breaks down, the system undergoes the Cassie-Wenzel transition showing the important role of the external pressure for the stability of underwater superhydrophobicity.

The rare-event method here employed also allows one to shed light on the origin of the irreversibility of the Wenzel state. Results show that, once the liquid fills the cavity, due to the finite value of the nucleation barrier $\Delta\Omega_{WC}$, it is entrapped in the Wenzel minimum until extreme negative pressures are reached. For the present geometry, at such pressures the Cassie state is also unstable and instantaneous bubble growth is expected. This result underscores that the recovery of superhydrophobicity is difficult to achieve for generic textures. However, it is possible to design textures, e.g., mimicking the Salvinia molesta [37], which maximize the range of pressures in which the superhydrophobic Cassie state exists [24].

Furthermore, the hysteresis cycle and the stability of the Cassie state can be modified by acting on the geometry of the surface. For instance, results show that it is possible to obtain three (meta)stable states by tuning the height of the T-shaped nanotextures. In summary, the present work suggests, on the one hand, that wetting of nanotextures is strongly history dependent and, on the other hand, that by designing the geometry and the chemistry of the nanotextures it is in principle possible to control its properties, including the stability of the superhydrophobic Cassie state.

ACKNOWLEDGEMENTS

The research leading to these results has received funding from the European Research Council under the European Union's Seventh Framework Programme (FP7/2007-2013)/ERC Grant agreement n. [339446]. We acknowledge PRACE for awarding us access

to resource FERMI based in Italy at Casalecchio di Reno.

---

[1] R. Wenzel, Ind. Eng. Chem. **28**, 988 (1936).

[2] A. Cassie and S. Baxter, Trans. Faraday Soc. **40**, 546 (1944).

[3] A. Lafuma and D. Quéré, Nat. Mater. **2**, 457 (2003).

[4] A. Checco, A. Rahman, and C. Black, Adv. Mater. **26**, 886 (2014).

[5] A. Tuteja, W. Choi, M. Ma, J. Mabry, S. Mazzella, G. Rutledge, G. McKinley, and R. Cohen, Science **318**, 1618 (2007).

[6] T. Krupenkin and J. Taylor, Nat. Commun. **2**, 448 (2011).

[7] S. Sharma and P. Debenedetti, Proc. Natl. Acad. Sci. USA **109**, 4365 (2012).

[8] S. Prakash, E. Xi, and A. Patel, Proc. Natl. Acad. Sci. USA **113**, 5508 (2016).

[9] J. Barrat and L. Bocquet, Phys. Rev. Lett. **82**, 4671 (1999).

[10] D. Gentili, G. Bolognesi, A. Giacomello, M. Chinappi, and C. M. Casciola, Microfluid. Nanofluid. **16**, 1009 (2014).

[11] J. Rothstein, Annu. Rev. Fluid Mech. **42**, 89 (2010).

[12] H. Kusumaatmaja, M. Blow, A. Dupuis, and J. Yeomans, Europhys. Lett. **81**, 36003 (2008).

[13] L. Lei, H. Li, J. Shi, and Y. Chen, Langmuir **26**, 3666 (2009).

[14] A. Checco, B. Ocko, A. Rahman, C. Black, M. Tasinkevych, A. Giacomello, and S. Dietrich, Phys. Rev. Lett. **112**, 216101 (2014).

[15] M. Xu, G. Sun, and C. Kim, Phys. Rev. Lett. **113**, 136103 (2014).

[16] P. Lv, Y. Xue, Y. Shi, H. Lin, and H. Duan, Phys. Rev. Lett. **112**, 196101 (2014).

[17] B. Lefevre, A. Saugey, J. Barrat, L. Bocquet, E. Charlaix, P. Gobin, and G. Vigier, J. Chem. Phys. **120**, 4927 (2004).

[18] N. Desbiens, I. Demachy, A. Fuchs, H. Kirsch-Rodeschini, M. Soulard, and J. Patarin, Angew. Chem.-Ger. Edit. **117**, 5444 (2005).

[19] L. Guillemot, T. Biben, A. Galarneau, G. Vigier, and É. Charlaix, Proc. Natl. Acad. Sci. USA **109**, 19557 (2012).

[20] R. Evans, U. M. B. Marconi, and P. Tarazona, J Chem. Soc. Farad. T. 2 **82**, 1763 (1986).

[21] L. Bruschi, G. Mistura, P. Phadungbut, D. Do, D. Nicholson, Y. Mayamei, and W. Lee, Langmuir **31**, 4895 (2015).

[22] H. Giesche, Part. Part. Syst. Character. **23**, 9 (2006).

[23] A. Marmur, Langmuir **24**, 7573 (2008).

[24] M. Amabili, A. Giacomello, S. Meloni, and C. Casciola, Adv. Mater. Interfaces **2** (2015).

[25] T. Liu and C. Kim, Science **346** (2014).

[26] L. Maragliano and E. Vanden-Eijnden, Chem. Phys. Lett. **426**, 168 (2006).

[27] A. Giacomello, S. Meloni, M. Chinappi, and C. Casciola, Langmuir **28**, 10764 (2012).

[28] A. Giacomello, S. Meloni, M. Müller, and C. Casciola, J. Chem. Phys. **142**, 104701 (2015).

[29] M. Amabili, E. Lisi, A. Giacomello, and C. Casciola, Soft Matter **12** (2016).

[30] D. Frenkel and B. Smit, *Understanding molecular simulation: from algorithms to applications*, Vol. 1 (Academic press, 2001).

[31] G. Martyna, M. Klein, and M. Tuckerman, J. Chem. Phys. **97**, 2635 (1992).

[32] S. Plimpton, J. Comp. Phys. **117**, 1 (1995).

[33] M. Bonomi, D. Branduardi, G. Bussi, C. Camilloni, D. Provasi, P. Raiteri, D. Donadio, F. Marinelli, F. Pietrucci, R. Broglia, *et al.*, Comput. Phys. Commun. **180**, 1961 (2009).

[34] A. Giacomello, M. Chinappi, S. Meloni, and C. Casciola, Phys. Rev. Lett. **109**, 226102 (2012).

[35] A. Luzar and K. Leung, J. Chem. Phys. **113**, 5836 (2000).

[36] A. Giacomello, M. Chinappi, S. Meloni, and C. Casciola, Langmuir **29**, 14873 (2013).

[37] W. Barthlott, T. Schimmel, S. Wiersch, K. Koch, M. Brede, M. Barczewski, S. Walheim, A. Weis, A. Kaltenmaier, A. Leder, *et al.*, Adv. Mater. **22**, 2325 (2010).

[38] O. Tricinci, T. Terencio, B. Mazzolai, N. Pugno, F. Greco, and V. Mattoli, ACS Appl. Mater. Interfaces **7**, 25560 (2015).

[39] This contact angle has been obtained setting the parameter c controlling the attractive term of the modified LJ potential to $c = 0.8$ of Eq. 1.

[40] A. Giacomello, L. Schimmele, and S. Dietrich, Proc. Natl. Acad. Sci. USA **113**, E262 (2016).

[41] H. Perrin, R. Lhermerout, K. Davitt, E. Rolley, and B. Andreotti, Phys. Rev. Lett. **116**, 184502 (2016).